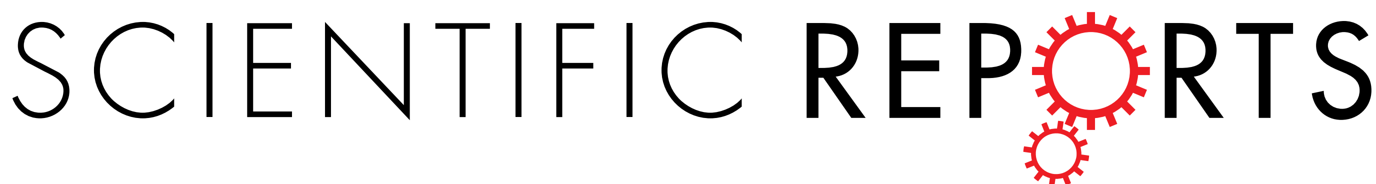

OPEN

# Low-Temperature Selective Growth of Tungsten Oxide Nanowires by Controlled Nanoscale Stress Induction

Received: 20 May 2015
Accepted: 28 September 2015
Published: 15 December 2015

**Hyungjoo Na, Youngkee Eun, Min-Ook Kim, Jungwook Choi & Jongbaeg Kim**

**We report a unique approach for the patterned growth of single-crystalline tungsten oxide ($WO_x$) nanowires based on localized stress-induction. Ions implanted into the desired growth area of $WO_x$ thin films lead to a local increase in the compressive stress, leading to the growth of nanowire at lower temperatures (600 °C vs. 750–900 °C) than for equivalent non-implanted samples. Nanowires were successfully grown on the microscale patterns using wafer-level ion implantation and on the nanometer scale patterns using a focused ion beam (FIB). Experimental results show that nanowire growth is influenced by a number of factors including the dose of the implanted ions and their atomic radius. The implanted-ion-assisted, stress-induced method proposed here for the patterned growth of $WO_x$ nanowires is simpler than alternative approaches and enhances the compatibility of the process by reducing the growth temperature.**

The wide direct band gap of tungsten oxide ($WO_x$)[1] makes it an attractive material for photoelectrochemical devices[2,3] and gas sensors[4]. The high surface to volume ratio and photon absorption efficiency of $WO_x$ nanowires[5] can be used to improve the performances of these devices, in particular the saturation photocurrent, the sensitivity, and the threshold field respectively of photoelectrochromical devices[6,7], gas sensors[8], and field-emission displays[9].

$WO_x$ nanowires are typically grown by vapor-solid (VS)[10–15], vapor-liquid-solid (VLS) synthesis[16,17], or hydrothermal synthesis[18,19]. In VS synthesis, a $WO_x$ layer is formed on a tungsten wire, tip, or filament, on which $WO_x$ nanowires grow under high-temperature annealing in an oxygen environment. Aligned nanowires can be grown using a KI catalyst by VLS synthesis at around 600–650 °C whereas hydrothermal synthesis is the preferred method for the large-scale production of $WO_x$ nanowires. Klinke *et al.*[20]. have developed an alternative method whereby $WO_x$ nanowires are grown by annealing $WO_3$/W substrates under hydrocarbon gas. The authors explain that in this case, the nanowires are the result of interfacial strain-induced carbide formation between the $WO_3$ and W layers. Elsewhere, the patterned growth of $WO_x$ nanowires has been demonstrated by Nakao and colleagues[21–23]; the $WO_x$ nanowires synthesized by annealing W/Cr thin films on Si substrates in a vacuum furnace with flowing oxygen gas are arranged into patterns using a micro heater or lift-off techniques. In this approach the nanowires extend via solid-phase growth from nanowire nuclei generated on the uneven W surface. To date however, although controlling the site and density of nanowires is a crucial factor for the practical application of nanowire devices, the growth of $WO_x$ nanowires in nanoscale patterns has seldom been investigated.

In our work, the driving force for the growth of nanowires is compressive stress induced from the difference in thermal expansion coefficients (TECs) and ion implantation. Compared to other growth methods of $WO_x$ nanowires such as VS-mechanism[10–15], a major benefit of our approach is high process compatibility due to low growth temperature. Moreover, this growth method does not require any precursor or catalyst.

In this study, by implanting ions into $WO_x$ thin films deposited on Si substrates, we have successfully synthesized $WO_x$ nanowires at 600 °C, 150 °C lower than for non-implanted films. This approach is based on stress-induced growth, whereby the compressive stress applied to thin films is relieved by the growth of nanowires. Compressive stress can be applied by oxidation-induced volume expansion[24,25], external loading[26], or by exploiting the difference between the TECs of the thin film and the substrate[27,28]. Here, the implanted ions generate additional compressive stress inside the film allowing nanowires to nucleate at lower temperatures (viz. 600 °C instead of 750 °C). The

School of Mechanical Engineering, Yonsei University, 50 Yonsei-ro, Seodaemun-gu, Seoul 120-749, Republic of Korea. Correspondence and requests for materials should be addressed to J.K. (email: kimjb@yonsei.ac.kr)

difference in the minimum nanowire growth temperature between the ion-implanted and non-implanted regions ensures that the patterns are grown in a site-specific manner, both on the micro- and nanoscale. Indeed, a single nanowire was successfully grown by reducing the ion-implanted area down to $50 \times 50\,\mathrm{nm}^2$, and wafer-scale growth of patterned nanowires is also possible. This is the first time the growth of $WO_x$ nanowires has been controlled on the nanoscale using localized compressive stress. Furthermore, this report explains the mechanisms governing the growth of $WO_x$ nanowires induced by the difference between the TECs of the thin film and the substrate.

## Results

**Stress-induced growth at lower temperature.** The nanowires were grown using a conventional two-step process. First, a 10-nm-thick $WO_x$ film was deposited on a (100) Si substrate by electron-beam evaporation using 99.9% $WO_3$ powder as an evaporation source. The substrate was then loaded into a furnace and annealed at temperatures above 700 °C for 20 min in a low-pressure environment with 100 sccm flowing $N_2$ (ca. 11 Torr). Supplementary Fig. 1 shows scanning and transmission electron microscopy (SEM and TEM) images of $WO_x$ nanowires synthesized without ion implantation at 700–950 °C. The high resolution TEM (HR-TEM) images of the nanowires grown at 750 °C are shown in Supplementary Fig. 1g, h. The length and density of the nanowires increases for growth temperatures up to 800 °C (Supplementary Fig. 1a–c), at which the nanowire density is maximal. On increasing the temperature to 900 °C the nanowires become more elongated but are less densely packed (Supplementary Fig. 1c–e). Supplementary Fig. 1f shows that no nanowires grow above 950 °C due to the crystallization of the thin film. Between 750 °C and 900 °C, the length of the nanowires is proportional to the growth temperature which in turn is directly related to the compressive stress. The selective-area electron diffraction (SAED) pattern (Supplementary Fig. 1g inset) highlights the crystallinity and the growth direction of the nanowires. Supplementary Fig. 1h shows that the nanowire is single crystalline with monoclinic $WO_x$ grown in [010] direction. Lattice constants of two planes, a = 0.377 nm and b = 0.467 nm, agree with a = 0.378 {010} and b = 0.459 {103} according to JCPDS Card No. 36–101.

These results confirm that it is the stress induced by the difference ($9.6 \times 10^{-6}\,\mathrm{m/mK^{-1}}$)[29] between the TECs of the $WO_x$ thin film ($12 \times 10^{-6}\,\mathrm{m/mK^{-1}}$) and the Si substrate ($2.4 \times 10^{-6}\,\mathrm{m/mK^{-1}}$) that leads to the growth of these nanowires. (Note that growth by oxidation-induced volume expansion of the metallic film, mentioned above, is not possible in the oxygen-less low-pressure $N_2$ environment used here.) These observations lead us further to the investigation of ion implantation as a means to increase the compressive stress in the thin film and grow nanowires at relatively low temperatures.

Figure 1 outlines the three steps involved in the implanted-ion-assisted, stress-induced method developed here. First, a 10-nm-thick $WO_x$ film is deposited on a bare Si wafer by electron-beam evaporation using 99.9% $WO_3$ powder as an evaporation source (Fig. 1a). We tested Ga, As, Ar, and $N_2$ ions to induce additional stress at reduced temperatures. For patterned growth characterization, As and Ga were used for ion implanter and focused ion beam, respectively. Ion implantation step was performed without heating the substrate. Figure 1b–d illustrates the similar steps with Ga ions implanted by a focused ion beam (FIB) into $WO_x$ films for nanoscale patterning. After ion implantation, the substrate is heated to increase the stress levels (Fig. 1c), and the $WO_x$ nanowires are synthesized on the ion-implanted nanoscale patterns (Fig. 1d). Figure 1e–g shows the patterned ion injection steps in the ion implanter using As, Ar, $N_2$ ions. Again, after implanting ions in selected areas using a shadow mask (Fig. 1e), the substrate is annealed (Fig. 1f). Compressive stress is induced from the difference in TECs and also from the implanted ions such that the threshold stress for the growth of $WO_x$ nanowires is reached in the ion-implanted region at a lower temperature than in the non-implanted surroundings (Fig. 1g). All the heating steps were conducted in a $N_2$ environment (ca. 11 Torr) at 600 °C for 60 min.

**Effect of dose and patterned growth.** Figure 2 shows SEM images of the $WO_x$ nanowires synthesized on $WO_x$ film using various doses of Ga ions implanted at 30 keV by FIB and following annealing at 600 °C for 60 min. The square patterns numbered 1–5 in Fig. 2a are $10 \times 10\,\mu\mathrm{m}^2$ in area and have implanted Ga doses of $1 \times 10^{15}$, $3 \times 10^{15}$, $5 \times 10^{15}$, $7 \times 10^{15}$, and $9 \times 10^{15}$ ions/cm$^2$, respectively. These results highlight the optimal ion dose to maximize the number density and length of the nanowires grown. The nanowires in pattern number 1 are short and relatively sparsely packed because the dose of $1 \times 10^{15}$ ions/cm$^2$ is insufficient to provide the compressive stress necessary to initiate growth. There are no nanowires in pattern number 5 ($9 \times 10^{15}$ ions/cm$^2$) because the $WO_x$ film becomes etched at higher doses. Long nanowires (>400 nm) are visible in patterns 2, 3, and 4 ($3 \times 10^{15}$, $5 \times 10^{15}$, and $7 \times 10^{15}$ ions/cm$^2$, respectively).

For nanoscale patterning, doses of $3 \times 10^{15}$, $5 \times 10^{15}$, and $7 \times 10^{15}$ ions/cm$^2$ where chosen, as shown in Fig. 2b (an enlarged view of pattern number 6 in Fig. 2a). Figure 2c shows a high magnification image of the nanoscale pattern obtained with a dose of $7 \times 10^{15}$ ions/cm$^2$, and corresponds to the region within the red square in Fig. 2b. The three sets of patterns in Fig. 2b are each composed of nanowires grown on five square areas covering (from top to bottom) $1000 \times 1000$, $500 \times 500$, $100 \times 100$, $75 \times 75$, and $50 \times 50\,\mathrm{nm}^2$. The nanowires are 10–20 nm in diameter and 300–1000 nm in length. The arrows numbered 1 and 2 in Fig. 2c respectively point out the three nanowires grown on the $100 \times 100\,\mathrm{nm}^2$ square and the single nanowire grown on the $75 \times 75\,\mathrm{nm}^2$ square. No nanowires are visible in Fig. 2c for the $50 \times 50\,\mathrm{nm}^2$ square; on the other hand, a single nanowire was successfully synthesized with this pattern size by annealing at 630 °C for 20 min, as shown in Supplementary Fig. 2.

Wafer-scale patterned growth of the $WO_x$ nanowires was realized using an ion implanter. As shown in Fig. 1b–d, the ions were implanted through a shadow mask placed on a 4 inch (10.16 cm) Si wafer coated with a 10-nm-thick $WO_x$ thin film. Figure 3 shows the nanowires grown after implanting As at $5 \times 10^{15}$ ions/cm$^2$ and 30 keV. Figure 3b shows an enlarged view of the corner of the square pattern shown in Fig. 3a, while Fig. 3c,d respectively show high magnification images of the center and the corner of the pattern.

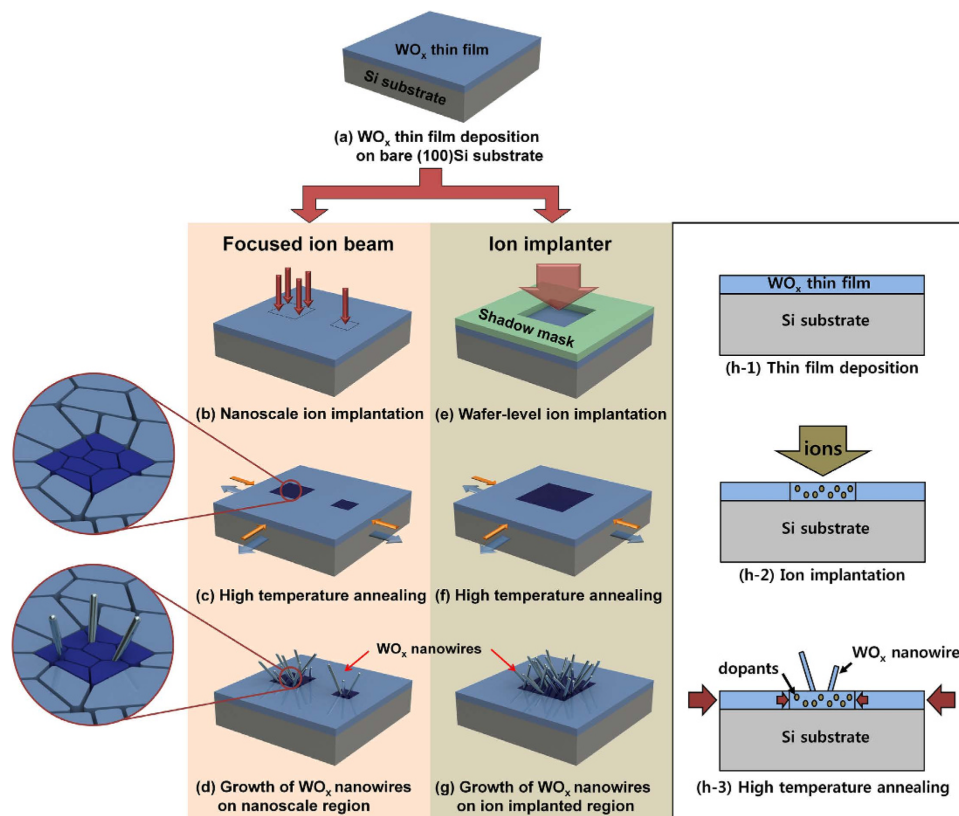


**Figure 1. Schematics of the different steps involved in the site-selective growth of $WO_x$ nanowires using the local stress induced by implanted ions.** (**a**) A $WO_x$ thin film is deposited on a (100) Si substrate by electron-beam evaporation. (**b–d**) Processing using a focused ion beam; (**b**) Ga ions are implanted in nanoscale areas; (**c**) the sample is annealed at 600 °C; (**d**) a small number of $WO_x$ nanowires grow in the Ga-ion-implanted nanoscale region. The magnified schematic depictions of the regions highlighted in (**c**,**d**) show the nanoscale morphology of the $WO_x$ thin films and nanowires in the ion-implanted (dark blue) regions where the grains are smaller. (**e–g**) Processing using an ion implanter; (**e**) As, Ar, or $N_2$ dopants are selectively implanted through a shadow mask onto the $WO_x$ thin film; (**f**) compressive stress arises from the difference between the thermal expansion coefficients of the thin film and the substrate during annealing at 600 °C in a furnace as in (**c**,**g**) $WO_x$ nanowires grow only in the ion-implanted region because the ions increase the compressive stress locally. (h1-3) Cross-sectional diagram of growth mechanism using compressive stress induced from the difference in TECs and ion implantation. Large red arrows indicate the compressive stress from difference in TECs; small red arrows indicate the additional compressive stress from ion implantation in the desired area. (h1-3) Cross-sectional diagram showing the growth of nanowires due to compressive stress. Large red arrows indicate the compressive stress from difference in TECs; small red arrows indicate the additional compressive stress from ion implantation in the desired area.

**Effect of dopants.** Because compressive stress plays a major role in the synthesis of these nanowires, implanting larger ions should facilitate nanowire growth. To investigate this effect, three bare Si wafers were coated with identical 10-nm-thick $WO_x$ films by electron-beam evaporation and different ions, As, Ar, and $N_2$ were implanted onto each of three wafers at $5 \times 10^{15}$ ions/cm$^2$ and 30 keV by an ion implanter. Figure 4a–c show SEM images, with magnified views inset, of the $WO_x$ nanowires—respectively 300–500 nm, 100–200 nm and $<100$ nm long—synthesized on the three different wafers after annealing at 600 °C for 60 min.

Figure 4d shows an HR-TEM image and the corresponding SAED pattern obtained from one of the $WO_x$ nanowires shown in Fig. 4a, grown by As implantation. As described above for the non-implanted results (Supplementary Fig. 1), the nanowire has a single-crystalline structure. The SAED patterns in Fig. 4d highlight growth in the (010) direction and the spacing of the lattice planes is visible in the magnified image (Fig. 4e). The energy dispersive X-ray spectrum in Fig. 4f reveals that the nanowire consists of 78% oxygen and 22% tungsten. The fact that the nanowire contains As less than the error range demonstrates that the implanted ions increase the compressive stress locally in the thin film without doping the resulting nanowires.

## Discussion

**Growth mechanism.** Nanowire growth mechanism used in our research is based on atomic diffusion enhanced by compressive stress in thin film from the difference in thermal expansion coefficient (TECs) between thin film and the substrate at high annealing temperature[27,28]. In this stress-induced method, $WO_x$ thin film has

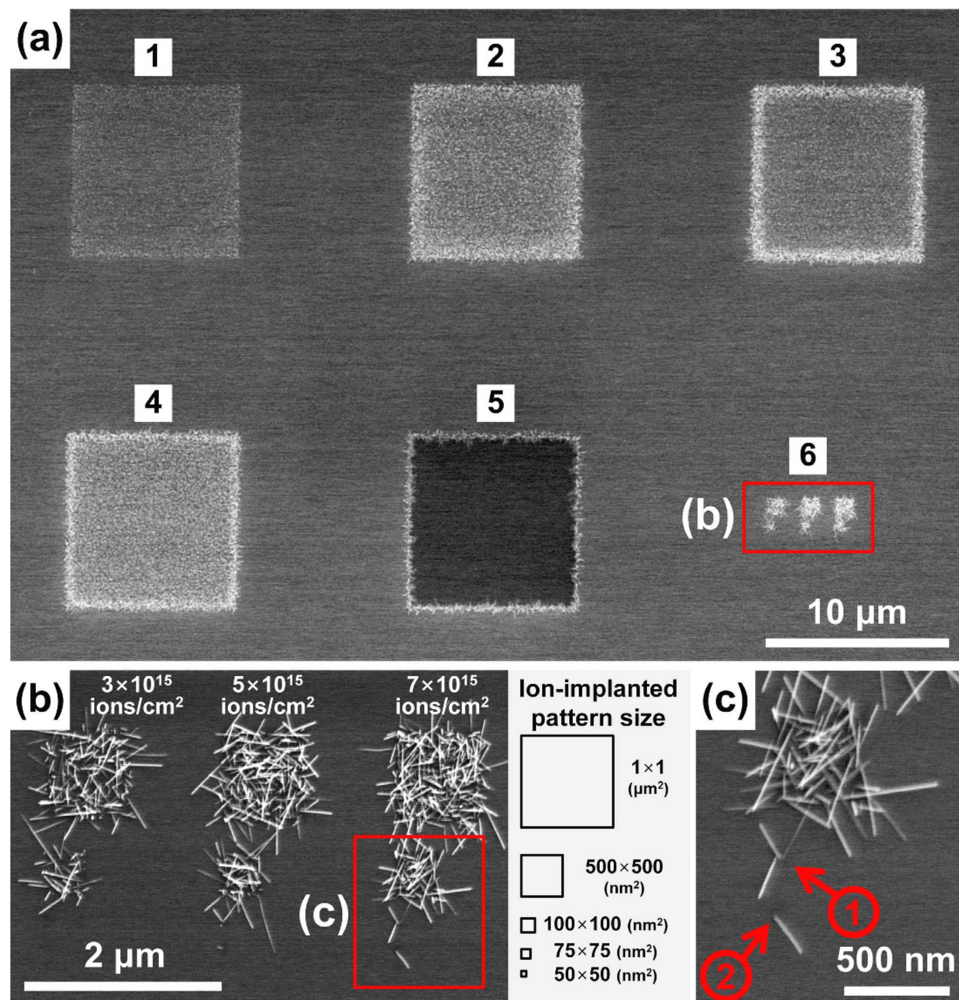


**Figure 2. Scanning electron micrographs of $WO_x$ nanowires grown in the Ga-ion-implanted regions of $WO_x$ thin films.** The samples were annealed at 600 °C for 60 min in a low-pressure environment under $N_2$ flow. (**a**) Square $10 \times 10\,\mu m^2$ patterns numbered 1 to 5 implanted using a 30 keV focused ion beam (FIB) with Ga doses of $1 \times 10^{15}$, $3 \times 10^{15}$, $5 \times 10^{15}$, $7 \times 10^{15}$, and $9 \times 10^{15}$ ions/cm$^2$, respectively. (**b**) Region number 6 in (a) contains three nanoscale patterns obtained with doses (from left to right) of $3 \times 10^{15}$, $5 \times 10^{15}$, and $7 \times 10^{15}$ ions/cm$^2$ implanted using a FIB in areas (from top to bottom) of $1000 \times 1000$, $500 \times 500$, $100 \times 100$, $75 \times 75$, and $50 \times 50$ nm$^2$, as depicted on the right of the panel. (**c**) High-magnification images of the region within the red rectangle in (**b**). The red arrows numbered 1 and 2 indicate the nanowires in the $100 \times 100$ and $75 \times 75$ nm$^2$ squares, respectively.

larger TECs than Si substrate (TEC of $WO_x$: $12 \times 10^{-6}$ m/mK$^{-1}$, TEC of Si: $2.4 \times 10^{-6}$ m/mK$^{-1}$) and is impeded to expand by the substrate, inducing compressive stress in it. In order to release the stress, nanowires are grown on the surface of the thin film by atomic diffusion at grain boundaries[27,28].

It is widely known that the implanted dopants also generate the compressive stress inside the target[30,31]. In our work, we utilized the compressive stress induced by both thermal mismatch and ion implantation for low temperature selective growth of $WO_x$ nanowires. As shown in Fig. 1(h), differences in TECs makes the entire thin film to be subjected to compressive stress, and implanted dopants generate additional compressive stress to facilitate the growth of nanowires only on the desired regions where ions are implanted. The magnitude of the compressive stress is proportional to annealing temperature, and there exist a threshold stress level and the corresponding temperature that initiates the growth of nanowires. In our experimental condition, the threshold temperature to produce sufficient compressive stress for nanowire growth is 750 °C without ion implantation, as shown in Supplementary Fig. 1. Thus at 600 °C, the stress level at non-implanted area is below the threshold stress and no nanowire is grown, while the ion-implanted region gets additional compressive stress from the implanted ions, which make the total stress level higher than the threshold stress for nanowire growth. Resultantly, $WO_x$ nanowires are grown only on the ion implanted area at a temperature lower than the threshold, 750 °C, as shown in the SEM images of Fig. 2.

As described previously[27,28], grain boundaries act as nucleation sites for nanowire growth; however, nanowires did not grow at all the grain boundaries in the ion-implanted area. It seems that the number of activated nucleation sites is somewhat sensitively dependent on the annealing temperature. Comparing the identical patterned area of

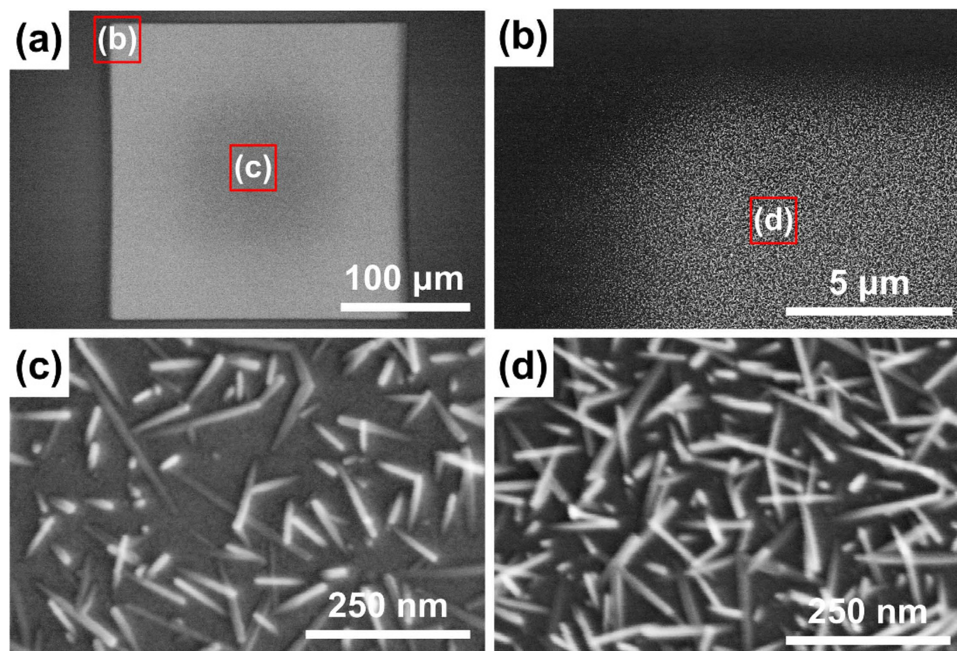


**Figure 3. Scanning electron micrographs of $WO_x$ nanowires grown on As-ion-implanted ($5 \times 10^{15}$ ions/$cm^2$) patterns obtained using an ion implanter operating at 30 keV.** The samples were then annealed at 600 °C for 60 min. (**a**) Patterned growth of $WO_x$ nanowires using a shadow mask, with (**b**) a magnified view of the top left corner of the square. High-resolution images showing nanowires grown (**c**) in the center and (**d**) in the corner of the pattern.

$100 \times 100\,nm^2$, when the annealing temperature is 600 °C, only 3 nanowires were grown (Fig. 2c), while 6 nanowires were observed at the annealing temperature of 630 °C (Supplementary Fig. 2b). To grow a single nanowire therefore, the annealing temperature and the implantation area and dose must all be carefully adjusted. Note furthermore that since the synthesis step was conducted at 600 °C, far below the melting point of W and $WO_x$, the VS and VLS mechanisms are clearly not involved in the growth of these nanowires.

Ion implantation facilitates the growth of nanowires through two different effects, thereby reducing the temperature required for their synthesis. Firstly, the volume of the implanted ions increases the compressive stress in the implanted region of the thin films[30,31]. Secondly, the ion implantation leads to the formation of smaller grains in the thin films during annealing, thereby reducing the activation energy for atomic diffusion at the grain boundaries[27,28]. During annealing, the grains in the as-deposited $WO_x$ thin films increase in size[32]; however, grain growth is hindered in the ion-implanted regions due to Zener pinning[33]. The relatively high surface-to-volume ratio of these smaller grains leads to a reduced activation energy for atomic diffusion[34], and as a result, nanowires grow in the ion-implanted regions at relatively low temperatures (see Fig. 1f,g).

**Effect of stress magnitude.** The increase in compressive stress in the films arising from the implanted ions is influenced by both the volume and the concentration of the implanted ions. The atomic/molecular radii of As, Ar, and $N_2$ dopants are 0.121, 0.096 and 0.07/0.109 nm (short/long), respectively[35], and we estimated their concentrations from the depth profiles measured by time-of-flight secondary ion mass spectrometry (TOF-SIMS) as shown in Supplementary Fig. 3. The projection ranges of As, Ar, and $N_2$ were 8 nm, 10 nm, and 7.8 nm, respectively, such that the peak concentration of the ions was formed within the thickness of the $WO_x$ thin film. However, since the doses were near the detection limit of the mass spectrometry, the concentrations of the implanted ions inside the thin film could not be measured accurately. For Ar and $N_2$, which are less readily ionized, the measurements could have been further impaired by these ions becoming trapped inside the film rather than forming chemical bonds with tungsten and oxygen atoms. With identical implantation dose and energy, the growth results varied depending on the ion species injected. Hence it could be concluded that heavier and larger dopants increase the compressive stress and lead to the growth of longer nanowires.

The nanowires in Figs 4a and 2b are of a similar length because the atomic radii of As (0.121 nm) and Ga (0.124 nm) are almost identical. The nanowires in Fig. 4c ($N_2$ implantation at $5 \times 10^{15}$ ions/$cm^2$) and Fig. 2a (Ga implantation at $1 \times 10^{15}$ ions/$cm^2$) are shorter because of the relatively low compressive stress arising respectively from the smaller atomic volume and the lower dose. These results show that the proposed method allows nanowires to be differently grown in length using different atomic sizes of various dopants. Additionally, the results obtained using Ar and $N_2$ dopants imply that the implanted ions have no catalytic effect on the growth of nanowires. In our test, not only the metallic dopants (Ga) and the semi-metallic dopants (As) but also the gaseous dopants (Ar and $N_2$) show similar results on the growth of nanowires when the growth temperature, pressure, and annealing time are identical. Therefore, it is unlikely for $WO_x$ to nucleate by dopant catalysts.

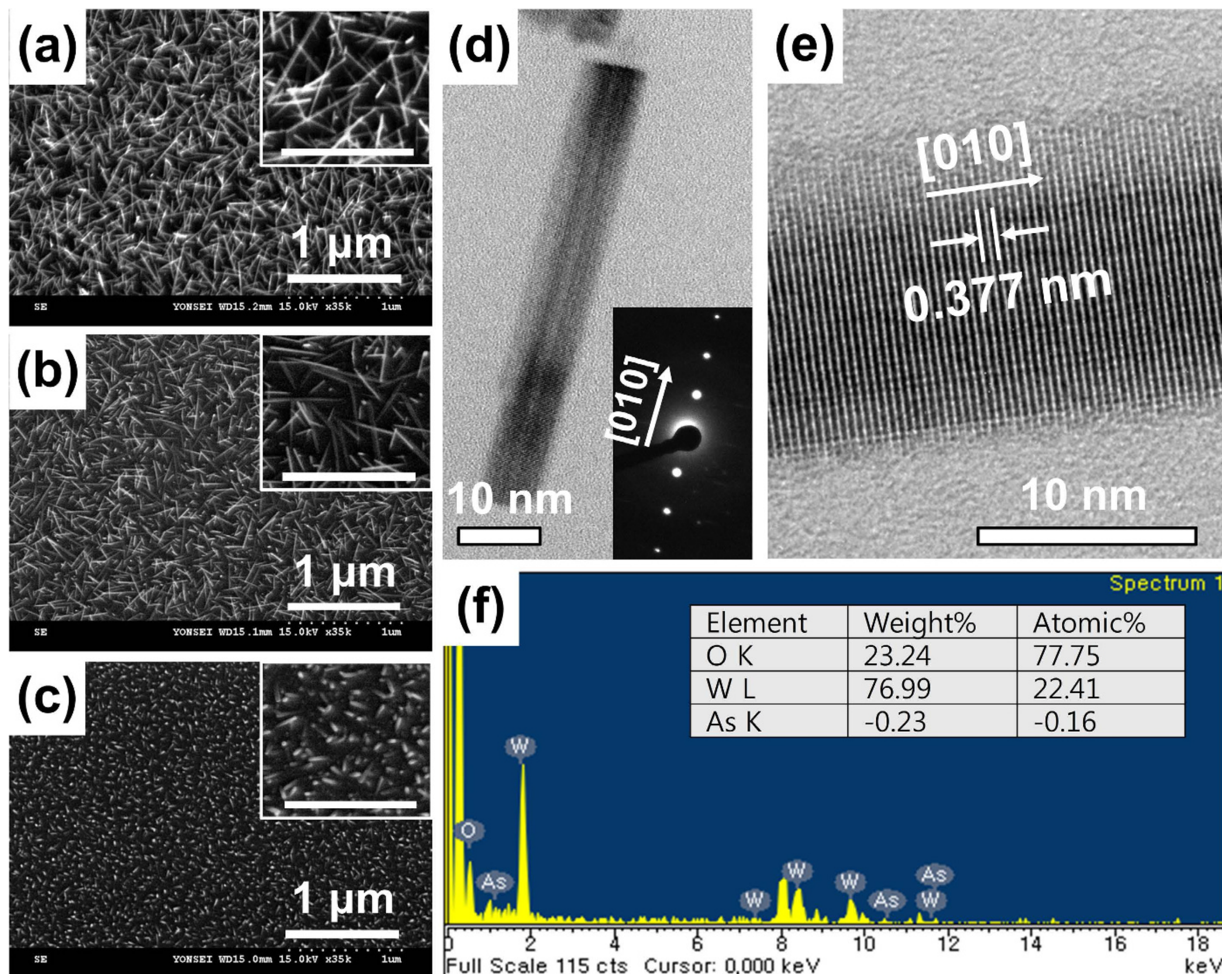


**Figure 4. $WO_x$ nanowires grown using an ion implanter with As, Ar, and $N_2$ dopants. All the samples were annealed at 600 °C for 60 min in a low-pressure environment under $N_2$ flow.** Scanning electron micrographs of the $WO_x$ nanowires grown on (**a**) As-, (**b**) Ar-, and (**c**) $N_2$-ion-implanted thin films. All dopants were implanted at 30 keV at a dose of $5 \times 10^{15}$ ions/cm$^2$. The insets in (**a**–**c**) show the corresponding high-magnification (scale bar: 500 nm) images. (**d**) A high-resolution scanning electron micrograph of a $WO_x$ nanowire grown on the As-ion-implanted sample shown in (**a**), with (inset) the corresponding selected area diffraction pattern. (**e**) An expanded view of the same nanowire clearly showing the lattice spacing and its axial direction. (**f**) Energy-dispersive X-ray spectrum showing the elemental content of the $WO_x$ nanowires grown on the As-implanted sample shown in (**a**).

In conclusion, we have successfully realized the scalable, site-specific growth of $WO_x$ nanowires at relatively low temperatures by exploiting the localized stress induced by ions implanted into $WO_x$ films. Experimental results show that the dopants increase the compressive stress locally, and that both their volume and dose have a direct impact on nanowire growth. That is, dopants with larger atomic radii lead to greater increases in stress, and thus to the growth of longer and more densely packed nanowires. Furthermore, since the extent of nanowire growth is governed by the size of the implantation area, reducing this down to the nanoscale allows a few or even a single isolated nanowire to be grown. The $WO_x$ nanowires synthesized in this way are single crystalline in structure, and the proposed stress-induced method does not require any precursor or catalyst. The reduction in the growth temperature achieved by the additional stress as well as the scalability of the process could render $WO_x$ nanowires amenable to a wider range of applications.

## Methods

**Thin Film Deposition.** For the $WO_x$ thin film deposition, 99.9% $WO_3$ powder was used as an evaporation source and (100) Si wafer was used as the substrate material. 10-nm-thick $WO_x$ film was electron-beam evaporated on to the Si wafer with a deposition rate of 0.5 Å/s.

**Ion Implantation.** (1) Using the FIB: Ga ions were implanted into $WO_x$ film with programmed patterns. The acceleration voltage, beam condition, and the beam size was 30 keV, 14 pA, and 14 nm, respectively. (2) Using the ion implanter: As, Ar, and $N_2$ dopants were implanted into the $WO_x$ film with an acceleration voltage of 30 keV.

**Annealing.** The specimens were heated in a furnace (Lindberg Blue M TF55030C) at low-pressure $N_2$ environment (ca. 11 Torr). Annealing temperature and time of un-implanted and implanted specimens were 700–900 °C for 20 min and 600 °C for 60 min, respectively.

## References


1. Bullett, D. W. Bulk and surface electron states in $WO_3$ and tungsten bronzes. *J. Phys. C: Solid State Phys*. **16,** 2197–2207 (1983).
2. Bechinger, C., Ferrere, S., Zaban, A., Sprague, J. & Gregg, B. A. Photoelectrochromic windows and displays. *Nature* **383,** 608–610 (1996).
3. Turyan, I. *et al.* Writing-Reading-Erasing on Tungsten Oxide Films using the Scanning Electrochemical Microscope. *Adv. Mater.* **12,** 330–333 (2000).
4. Meixner, H., Gerblinger, J., Lampe, U. & Fleischer. M. Thin-film gas sensors based on semiconducting metal oxides. *Sens. Actuators, B* **23,** 119–125 (1995).
5. Serrano, E., Rus, G. & Garcı´a-Martı´nez, J. Nanotechnology for sustainable energy. *Renewable Sustainable Energy Rev.* **13,** 2373–2384 (2009).
6. Liao, C.-C., Chen, F.-R. & Kai, J.-J. $WO_{3-X}$ nanowires based electrochromic devices. *Sol. Energ. Mat. Sol. C.* **90,** 1147–1155 (2006).
7. Su, J., Feng, X., Sloppy, J. D., Guo, L. & Grimes, C. A. Vertically aligned $WO_3$ nanowire arrays grown directly on transparent conducting oxide coated glass: synthesis and photoelectrochemical properties. *Nano Lett.* **11,** 203–208 (2011).
8. Rout, C. S., Govindaraj, A. & Rao, C. N. R. High-sensitivity hydrocarbon sensors based on tungsten oxide nanowires. *J. Mater. Chem.* **16,** 3936–3941 (2006).
9. Li, Y., Bando, Y. & Golberg, D. Quasi-aligned single-crystalline $W_{18}O_{49}$ nanotubes and nanowires. *Adv. Mater.* **15,** 1294–1296 (2003).
10. Gu, G., Zheng, B., Han, W. Q., Roth, S. & Liu, J. Tungsten oxide nanowires on tungsten substrates. *Nano Lett.* **2,** 849–851 (2002).
11. Liu, Z., Bando, Y. & Tang, C. Synthesis of tungsten oxide nanowires. *Chem. Phys. Lett.* **372,** 179–182 (2003).
12. Liu, K., Foord, D. T. & Scipioni, L. Easy growth of undoped and doped tungsten oxide nanowires with high purity and orientation. *Nanotechnology* **16,** 10–14 (2005).
13. Cho, M. H. *et al.* Evolution of tungsten-oxide whiskers synthesized by a rapid thermal-annealing treatment. *J. Vac. Sci. Technol., B* **22,** 1084–1087 (2004).
14. Chang, M.-T. *et al.* Nitrogen-doped tungsten oxide nanowires: low-temperature synthesis on si, and electrical, optical, and field-emission properties. *Small* **3,** 658–664 (2007).
15. Baek, Y. & Yong, K. Controlled growth and characterization of tungsten oxide nanowires using thermal evaporation of $WO_3$ powder. *J. Phys. Chem. C* **111,** 1213–1218 (2007).
16. Qi, H., Wang, C. & Liu, J. A Simple Method for the Synthesis of Highly Oriented Potassium-Doped Tungsten Oxide Nanowires. *Adv. Mater.* **15,** 411–414 (2003).
17. Hong, K., Yiu, W., Wu, H., Gao, J. & Xie, M. A simple method for growing high quantity tungsten-oxide nanoribbons under moist conditions. *Nanotechnology* **16,** 1608–1611 (2005).
18. Song, X., Zhao, Y. & Zheng, Y. Hydrothermal synthesis of tungsten oxide nanobelts. *Mater. Lett.* **60,** 3405–3408 (2006).
19. Huang, K. *et al.* Controllable synthesis of hexagonal $WO_3$ nanostructures and their application in lithium batteries. *J. Phys. D: Appl. Phys*. **41,** 155417 (2008).
20. Klinke, C., Hannon, J. B., Gignac, L., Reuter, K. & Avouris, P. Tungsten oxide nanowire growth by chemically-induced strain. *J. Phys. Chem. B* **109,** 17787–17790 (2005).
21. Nagato, K. *et al.* Local Synthesis of tungsten oxide nanowires by current heating of designed micropatterned wires. *Appl. Phys. Express* **1,** 014005 (2008).
22. Kojima, Y., Kasuya, K., Nagato, K., Hamaguchi, T. & Nakao, M. Solid-phase growth mechanism of tungsten oxide nanowires synthesized on sputtered tungsten film. *J. Vac. Sci. Technol. B* **26,** 1942–1947 (2008).
23. Furubayashi, M., Nagato, K., Moritani, H., Hamaguchi, T. & Nakao, M. Field emission properties of discretely synthesized tungsten oxide nanowires. *Microelectron. Eng.* **87,** 1594–1596 (2010).
24. Hoffman, E. N., Barsoum, M. W., Wang, W., Doherty, R. D. & Zavaliangos, A. On the spontaneous growth of soft metallic whiskers. Proc. 51st IEEE Holm Conf. on Electrical Contacts pp 121–126 (2005).
25. Kaura, M. *et al.* Growth and branching of CuO nanowires by thermal oxidation of copper. *J. Cryst. Growth* **289,** 670–675 (2006).
26. Fisher, R. M., Darken, L. S. & Carroll, K. G. Accelerated growth of tin whiskers. *Acta Metall.* **2,** 368–373 (1954).
27. Shim, W. *et al.* On-film formation of bi nanowires with extraordinary electron mobility. *Nano Lett.* **9,** 18–22 (2009).
28. Ham, J. *et al.* Direct growth of compound semiconductor nanowires by on-film formation of nanowires: bismuth telluride. *Nano Lett.* **9,** 2867–2872 (2009).
29. Tokunaga, T. *et al.* Growth and structure analysis of tungsten oxide nanorods using environmental TEM. *Nanoscale Res. Lett.* **7,** 85 (2012).
30. Kalyanasundaram, N., Moore, M. C., Freund, J. B. & Johnson, H. T. Stress evolution due to medium-energy ion bombardment of silicon. *Acta Mater.* **54,** 483–491 (2006).
31. Rajaram, M. & Friebele, E. J. Effects of radiation on the properties of low thermal expansion coefficient materials: a review. *J. Non-Cryst. Solids* **108,** 1–17 (1989).
32. Jayatissa, A. H., Chengb, S. T. & Gupta, T. Annealing effect on the formation of nanocrystals in thermally evaporated tungsten oxide thin films. *Mater. Sci. Eng. B* **109,** 269–275 (2004).
33. Doherty, R. D. *et al.* Current issues in recrystallization: a review. *Mater. Sci. Eng., A-Struct*. **238,** 219–274 (1997).
34. Jiang, Q., Zhang, S. H. & Li, J. C. Grain size-dependent diffusion activation energy in nanomaterials. *Solid State Commun.* **130,** 581–584 (2004).
35. Pyykko, P. & Atsumi, M. Molecular single-bond covalent radii for elements 1–118. *Chem. Eur. J.* **15,** 186–197 (2009).


## Acknowledgements

H.N. and Y.E. contributed equally to this work. This research was supported by the Basic Science Research Program through the National Research Foundation of Korea (NRF) funded by the Ministry of Education, Science and Technology (2012R1A1A2043661). This work was also supported by the Smart IT Convergence System Research Center funded by the Ministry of Education, Science and Technology as a "Global Frontier Project" (2012M3A6A6054201) and Korea Ministry of Environment as "The Converging Technology Program". The authors thank Mr. Kisik Koh for the help in operating FIB.

## Author Contributions

H.N. and Y.E. contributed equally to this work. H.N., Y.E., M.-O.K., J.C. and J.K. discussed the experimental design and results. H.N., Y.E. and J.K. drafted the manuscript. J.K. conceived and supervised the research and revised the manuscript. All the authors read and approved the final manuscript.

## Additional Information

**Supplementary information** accompanies this paper at http://www.nature.com/srep

**Competing financial interests:** The authors declare no competing financial interests.

**How to cite this article**: Na, H. *et al.* Low-Temperature Selective Growth of Tungsten Oxide Nanowires by Controlled Nanoscale Stress Induction. *Sci. Rep.* **5**, 18265; doi: 10.1038/srep18265 (2015).

This work is licensed under a Creative Commons Attribution 4.0 International License. The images or other third party material in this article are included in the article's Creative Commons license, unless indicated otherwise in the credit line; if the material is not included under the Creative Commons license, users will need to obtain permission from the license holder to reproduce the material. To view a copy of this license, visit http://creativecommons.org/licenses/by/4.0/